“True” colour presentation of suburban areas from colour-infrared aerial photos

Thomas Knudsen

National Survey and Cadastre—Denmark
8 Rentemestervej
DK-2400 Copenhagen NV
Denmark

`http://research.kms.dk/~thk`
`thk@kms.dk`

Thomas Knudsen: “True” colour presentation of suburban areas from colour-infrared aerial photos

National Survey and Cadastre—Denmark, technical report series number 20, published 2003-03

ISSN: 0908-2867
ISBN: 87-7866-367-9

See page 36 for a list of all technical reports

This report is available from URL `http://research.kms.dk/~thk/pubs/`

Abstract

This report adresses the problem of true colour presentation of colour-infrared photogrammetric aerial imagery.

This is important because colour-infrared photos are superior to true colour photos in applications of automated change detection for topographic map updates, while true colour photos are superior to colour-infrared photos for presentation and visual interpretation purposes.

The focus of the report is on the first step of a two step procedure, where a first guess (from a least squares adjusted linear model) is later refined using heuristics.

A number of models, using different image channels as basis functions, and splitting the phase space into 1, 2, and 8 sub-domains, are computed and tested.

It is concluded that a full domain model based directly on the near-infrared, red, and green channels from the colour-infrared photo is sufficient: the more complex models gains little extra.

keywords: colour transformation, aerial photography, colour-infrared, true colour, photogrammetry, automatic change detection

List of Figures

Contents

Chapter 1

Introduction

Due to the large difference in reflectivity in near-infrared wavelengths between vegetation and man made materials, colour-infrared aerial photos are in general superior to their true colour counterparts with regard to automated detection of topographically important man made objects (Knudsen and Olsen, 2003, 2002; Petzold, 2000; Petzold and Walter, 1999; Walter, 2000).

This makes it tempting to replace the true colour photo flights traditionally used for maintenance of topographical data bases, with colour-infrared missions.

The colour formation process in colour-infrared photography is outlined in figure 1.1. It is quite different from true colour photography, but in brief, the resulting colour-infrared positive image (i.e. after reversal processing of the negative film) represents near-infrared light by red dyes, red light by green dyes, and green light by red dyes. Blue light is filtered out with a yellow filter before the light enters the aerial camera.

This cycling of the colour representation makes colour-infrared photos less suitable for presentation purposes, and for visual analysis by stereo analysts: colour-infrared photos look dramatically different from true colour photos (vegetation shows up in red, red bricks in yellow, et cetera), invalidating established visual interpretation experience.

Due to the remarkable adaptivity of the human visual processing chain we may, however, expect that even a semi-decent colour reconstruction will be enough to greatly enhance the interpretability of the colour-infrared photos. This will give us the best of both worlds: the colour-infrared photo for automated tasks and the colour-reconstructed photo for human interpretation.

In principle we have most of the information needed to do a simple and fully deterministic transform of colour-infrared to true colour: the colour-infrared photos include red and green channels leaving just the blue spectral range uncovered. And as the human eye is least sensitive to blue light, one may expect this to be a minor problem.

Practical experience, however, shows that taking the red and green channels from the colour-infrared photo and ignoring the blue range, does *not* result in satisfactory results (cf. figure 4.1, page 13).

The main hypothesis behind this work is that *using a (least-squares adjusted) linear transform, followed by spectral corrections based on ad-hoc heuristics, it is possible to generate a pseudo-true colour representation of a colour-infrared photo which is fully satisfactory for a stereo analyst.* But the material presented here is not an attempt to deliver an end-to-end proof of this hypothesis; rather to take the first step by evaluating different linear transforms in order to find the best possible base for the final ad-hockery, which will be presented in forthcoming work (Knudsen, in preparation).

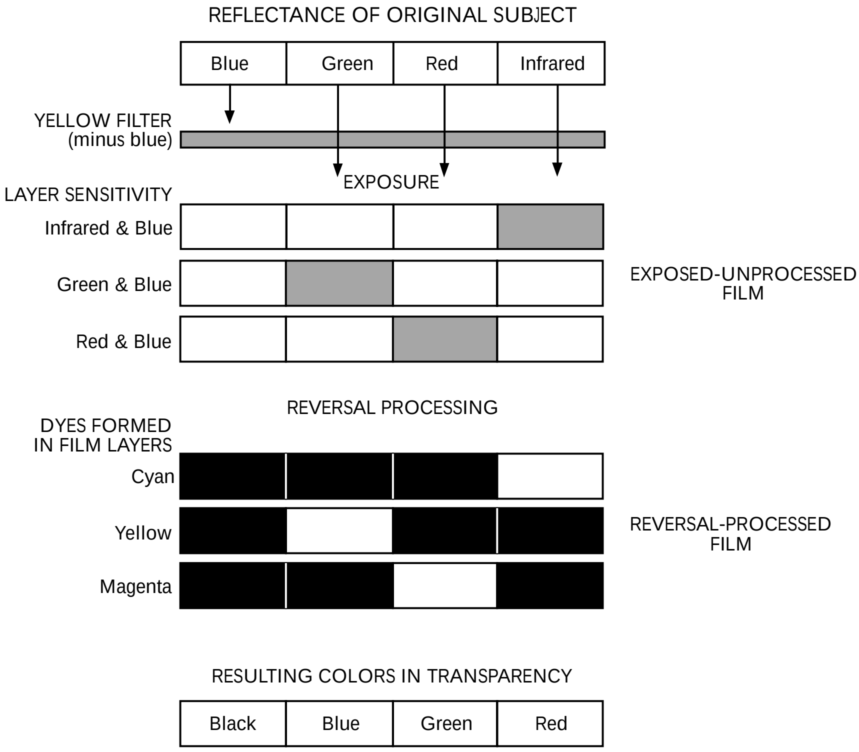

Figure 1.1: The colour formation process in colour-infrared film (reproduced from Kodak (2002))

The areas of primary interest are of suburban type. Suburbs cover large areas compared to inner cities, and suburban topography often change due to building reconstructions, new buildings, new roads, etc. This leads to the necessity of much update for suburban topographic map/GIS databases (rural zones cover even larger areas than suburbs, but they usually contain much fewer buildings, roads, and other GISwise important objects, making rural database updates much simpler than suburban).

So the main objective of this work is to *compute a number of linear transforms for deriving an artificial blue channel in suburban areas, and to investigate the relative merits of those transforms*. The *a priori* expectation is that a minor extension to the simple $blue = 0$ scheme will take us a long way, and that computationally more expensive approaches adds minor gains only.

Chapter 2

Data

The primary input data investigated are suburban subareas of the aerial photo test data set presented by Knudsen et al. (2000). The test data set contains colour-infrared (CIR) and true colour aerial photos of an urban-to-suburban area in Lyngby, 15 km north of Copenhagen, Denmark. The original colour-infrared photos were shot (using Kodak AEROCHROME III-1443 film (Kodak, 2002)) at a nominal scale of 1:25000, and scanned at a resolution of $21\mu m$, for a nominal ground resolution of approximately $0.5m$ (see appendix A for spectral details).

To facilitate the computation of linear transformations from the three channels available in CIR photos to the fourth (blue) channel, a true four channel photo is used (cf. figure 2.1). This photo covers a urban/suburban area in Hartford, Connecticut, shot using an ADAR 5500 digital airborne sensor system, and provided by Positive Systems, Inc. (see appendix B for details).

Figure 2.1: Four channel image (near infrared, red, green, blue) of Hartford, Connecticut, obtained on 1999-05-01, using the ADAR System 5500 and provided by Positive Systems, Inc.

Upper panel: true colour representation using the red, green and blue channels.

Lower panel: colour-infrared representation using the near infrared, red and green channels. This (and the following) figure follows the traditional presentation mode for CIR photos: infrared channel is shown in red, red channel in green, and green channel in blue, representing vegetation in red shades, since chlorophyll is a very efficient reflector of near-infrared light

Figure 2.2: Suburban test area 1: true colour photo from 2000-03-24

Figure 2.3: Suburban test area 1: colour-infrared photo from 2000-06-10.

Chapter 3

Method

3.1 Baseline method

The method used here is simply to compute the linear transformations which, in the least squares sense, gives the best reproduction of the blue channel from the near infrared (N), red (R) and green (G) channels and/or additional channels derived from N, R and G. A similar method was used by Cardei (1999) in a model study aiming at image compression and recovery of lost spectral channels. In a notation following Cardei we seek the column vector W,

$$W = [N \quad R \quad G]^{*} \cdot B$$

where N, R, G, and B are column vectors containing the image pixels (rowwise concatenated into a single column), such that $[N \quad R \quad G]$ is a n rows by 3 columns matrix, where n is the total number of pixels in the image. The * operator denotes the pseudo-inverse. Hence, W is the least squares solution minimizing

$$\sum_{\text{all pixels}} (B - [N \quad R \quad G] \cdot W)^2$$

Least squares models were computed for a number of different channel combinations, described in chapter 4, below.

Cardei (1999) argued that from a colour constancy point of view polynomial terms (e.g. R^2, $R \times G$, etc.) should be avoided as basis functions in the data set, since they introduce a brightness sensitivity into the hue of the restored pixel (with linear terms only, the restored channel value becomes a weighted average of the remaining channel values). The task at hand here is, however, very different from the channel dropout case studied by Cardei, so the "strictly linear" recommendation is not followed rigorously.

3.2 Quality indicators for the fitted parameters

For each model a set of 5 descriptive statistics were generated, in order to characterize the skill of the model with respect to recovery of the original blue channel. The sets of statistics are presented as rows of 5 numbers in chapter 4, below (and summarized in appendix C, page 28). The 5 numbers are as follows:

1. *minimum deviation:* the minimum deviation between a computed blue channel pixel value and the original blue channel pixel value. This number is almost always 0, denoting that at least one pixel is perfectly recovered.

2. *mean absolute deviation:* the mean (over all pixels) of the absolute deviation between the computed blue channel pixel values and the original blue channel pixel values.

3. *maximum deviation:* the maximum deviation between a computed blue channel pixel value and the original blue channel pixel value. This number is almost always fairly large.

4. *standard fit:* the root-mean-square (over all pixels) of the difference between the computed blue channel pixel values and the original blue channel pixel values.

5. *PSNR:* the peak signal to noise ratio, here using the definition $\mathrm{PSNR} = 20 \times \log_{10}(1/\mathrm{rms})$, measuring the ratio (in dB) between the maximum signal value $(= 1)$ and the root-mean-square (over all pixels) of the difference between the computed blue channel pixel values and the original blue channel pixel values. An increase of 20 dB corresponds to a ten-fold decrease in the rms difference.

The quality of the models with respect to restoration of the true colour of additional (three channel) data sets is done by visual inspection only.

3.3 Simplest models

The simplest possible model is the one with $W = [0 \quad 0 \quad 0]$, i.e. with the blue channel set to 0 throughout the image. This case is presented in section 4.1.

The simplest non-trivial model comes from a least-squares regression of the blue channel versus the red and green channels in the true colour image in figure 2.2. This case is presented in section 4.2.

A (hopefully) better model comes when doing the regression of the blue channel against the near-infrared, red and green channels from the four channel image in figure 2.1. This case is presented in section 4.3.

3.4 Octant splitting in phase space

To investigate more parameter rich models, a number of models were computed using separate parameter regressions in the 8 octant domains of the N-R-G phase space. The octant index of a pixel is defined as $O = (N > 1/2) + 2 \times (R > 1/2) + 4 \times (G > 1/2)$.

The octant splitting models are presented in sections 4.6–4.8.

3.5 Vegetation index and bitant splitting

The normalized difference vegetation index (NDVI), defined by

$$NDVI = \frac{N - R}{N + R}$$

is a simple, classic, and not entirely unproblematic measure of the degree of vegetation surface cover. The standard interpretation is that $NDVI > 0$ indicates vegetation covered areas.

In a number of the models presented in chapter 4, the NDVI was used [1] in the set of basis functions—either as an extra channel or as a replacement for the near-infrared channel.

In other models, the NDVI was used to define a bitant domain-splitting, where the bitant index is defined as $O = (NDVI > 1/2)$, i.e. a bitant index of 0 indicates non-vegetation, while a bitant index of 1 indicates vegetation.

The bitant splitting models are presented in sections 4.9–4.11.

[1] strictly speaking, the index used was the Infrared Percentage Vegetation Index (IPVI), which translates to NDVI through the relation $IPVI = (NDVI + 1)/2$ (Crippen, 1990)

Chapter 4

Results

The results of the experiments are presented on the following pages in a uniform setup with one transformation experiment per page.

The main element of each page is the image, showing the result of the transformation on the scene presented in figure 2.3, page 9 (the experiments have been re-run over several other test areas—the results presented here are typical).

After a brief description of the transformation (esp. input channels), and its relative merits (from a subjective visual inspection), the numerics are quoted, in a format which is a slightly edited version of the output from the fitting routine shown in appendix D.

The actual model is designated by an identifier of the form `Wx`. The `W` indicates that we are looking at a weight function. The `x` is a single capital letter or arabic numeral, assigned merely for distinction, and in no particular order.

Finally, the statistical vector, described in section 3.2, is reproduced with a set of headers (min, mean, max, rms, PSNR) with evident meaning.

The numerical results of all experiments are summarized in a slightly more uniform setup in appendix C

Figure 4.1: Red and green channel from figure 2.3. Blue is set to 0

4.1 No blues: B = 0

Red and green channel from the CIR photo in figure 2.3, page 9. Setting the blue channel to zero results (not surprisingly) in a visually very unpleasing appearance: the area seems to suffer from an attack of a heavy yellow haze.

The PSNR is below 10, reflecting that the true blue colour differs significantly from zero.

```
W0 = [0  0  0]'

            min      mean     max       rms     PSNR
W0        0.0000   0.2801   1.0000   0.3321   9.5751
```

Figure 4.2: Blue is a linear combination of red and green from figure 2.3

4.2 B(R,G)

Red and green channel from the CIR photo in figure 2.3, page 9. Blue is generated from a linear combination of the red, and green channels. The transformation used here was based on a regression of blue versus red and green bands from the true colour image of the same area shown in figure 2.2, page 8

This results in a dramatic increase in PSNR, which is more than doubled compared to the blue=0 case.

There are, however, still remnants of the yellow haze effect.

```
WB = [0  0.1757  0.4430]'

           min      mean     max       rms      PSNR
WB stats  0.0000   0.0725   0.7594   0.0979   20.1879
```

Figure 4.3: Blue is a linear combination of all bands from figure 2.3

4.3 B(N,R,G)

Red and green channel from the CIR photo in figure 2.3, page 9. Blue is generated from a linear combination of the infrared, red, and green channels. The transformation used here was based on a regression of blue versus infrared, red and green from the 4 channel photos shown in figure 2.1, page 7

This blows away the last remnants of yellow haze—perhaps at the expense of a more dull colour in the vegetation covered areas.

We also get another significant rise of 5.6 dB in PSNR, which is now close to 25.8 dB

```
WC = [-0.1423  0.2415  0.7007]'

            min      mean     max       rms      PSNR
WC stats  0.0000   0.0360   0.6881   0.0513   25.7982
```

See also

- Octant version: section 4.6, page 18
- Bitant version: section 4.9, page 21

Figure 4.4: Blue is a linear combination of all bands and NDVI from figure 2.3

4.4 B(N,R,G,NDVI)

Red and green channel from the CIR photo in figure 2.3, page 9. Blue is generated from a linear combination of the infrared, red, and green channels, combined with the NDVI based on the red and near-infrared channels. The transformation used here was based on a regression of blue versus infrared, red and green from the 4 channel photos shown in figure 2.1, page 7

There is only a slight visible difference between this image and the previous: slightly less dull vegetation, and slightly better reproduction of red tile roofs. The PSNR is up by another 0.4 dB.

```
WE = [-0.1248  0.3018  0.5683  0.0612]'
```

```
            min      mean     max       rms      PSNR
WE stats  0.0000   0.0305   0.6581   0.0490   26.2038
```

See also

- Octant version: section 4.7, page 19
- Bitant version: section 4.10, page 22

Figure 4.5: Blue is a linear combination of red, green and NDVI from figure 2.3

4.5 B(R,G,NDVI)

Red and green channel from the CIR photo in figure 2.3, page 9. Blue is generated from a linear combination of the red, and green bands of the original CIR photo combined with the NDVI based on the red and near-infrared channels. The PSNR is 0.45 dB lower, but there is no visible difference between this image and the $B = \mathrm{B}(N,R,G)$ case presented in section 4.3.

```
W1 = [0.4528  0.3024  0.0801]'

             min      mean     max       rms      PSNR
W1 stats  0.0000   0.0357   0.6684   0.0540   25.3583
```

See also

- Bitant version: section 4.11, page 23

Figure 4.6: Blue is a linear combination in octants of all bands from figure 2.3

4.6 B(N,R,G)—octant split

Red and green channel from the CIR photo in figure 2.3, page 9. Blue is generated from a linear combination of the near-infrared, red, and green channels.

The regression was carried out independently in each octant.

There is some visible difference between this image and the previous one: the vegetation covered areas are slightly less dull in appearance (resembling the $B = \mathrm{B}(N,R,G,NDVI)$, section 4.4).

The PSNR is 0.8 dB higher than in the $B = \mathrm{B}(N,R,G)$ case presented in section 4.3.

```
octant    0         1         2         3         4         5         6         7
WF =
N     -0.1357    0.0336   -0.4949    0.0185   -0.2250   -0.1249   -0.2704   -0.2654
R      0.0755    0.5058    0.5392    0.1383    0.7801    0.5494    0.1163    0.4559
G      0.8755    0.1589    0.6562    0.5893    0.2533    0.3406    0.8638    0.6217

            min      mean      max       rms      PSNR
WF stats  0.0000   0.0301   0.6706   0.0468   26.5924
```

Figure 4.7: Blue is a linear combination in octants of all bands+NDVI from figure 2.3

4.7 B(N,R,G,NDVI)—octant split

Red and green channel from the CIR photo in figure 2.3, page 9. Blue is generated from a linear combination of the red, and green channels, combined with the NDVI based on the red and near-infrared channels.

The regression was carried out independently in each octant.

The PSNR is 1.1 dB higher than in the $B = \mathrm{B}(N,R,G)$ octant case presented in section 4.6 and 2.0 dB higher than the plain $B = \mathrm{B}(N,R,G)$ case presented in section 4.3. It is 1.6 dB higher than the plain $B = \mathrm{B}(N,R,G,NDVI)$ case (section 4.4). There is, however, no visible difference between this case and the $B = \mathrm{B}(N,R,G)$ octant case.

```
octant    0         1         2         3         4         5         6         7
WG =
N     -0.0742    0.0377   -0.5012    0.0102   -0.1321   -0.1612   -0.2711   -0.1894
R      0.3932    0.3775    0.5534    0.1796    0.5982    0.7421    0.1114    0.7137
G      0.3849    0.1246    0.6611    0.6213    0.1865    0.3964    0.8639    0.8037
NDVI   0.0992    0.1512   -0.0128   -0.0666    0.1537   -0.2220    0.0054   -0.7213

          min       mean      max       rms       PSNR
WG stats  0.0000    0.0240    0.7108    0.0409    27.7721
```

Figure 4.8: Blue is a linear combination in octants of bands generated from figure 2.3

4.8 B(N,R,G,NDVI...)—octant split

Red and green channel from the CIR photo in figure 2.3, page 9. Blue is generated from a linear combination of the near-infrared, red, and green channels of the original CIR photo, supplemented by the NDVI based on the red and near-infrared channels, and the channel products $N \times R$, $R \times G$, $G \times N$, $N \times N$, $R \times R$, $G \times G$.

The regression was carried out independently in each octant.

The PSNR is 0.4 dB higher than in the $B = \mathrm{B}(N, R, G, NDVI)$ octant case (section 4.7) and 2.0 dB higher than the plain $B = \mathrm{B}(N, R, G, NDVI)$ case (section 4.4). There is, however, no visible difference between this case and the $B = \mathrm{B}(N, R, G)$ octant case.

octant	0	1	2	3	4	5	6	7
W2 =								
N	0.1589	0.0457	1.3731	-0.5297	-0.0757	-1.0522	0.5289	0.3732
R	0.3393	-0.4199	-0.2935	1.1845	1.3166	1.2913	0.5662	-2.5408
G	0.3375	0.0690	0.1773	0.4259	0.4075	1.3465	-0.6154	0.0836
N*R	-0.1046	0.0487	-1.6563	-0.1005	-1.1329	0.1757	-2.3948	0.3172
R*G	1.5717	1.5754	3.8368	1.2009	2.5794	0.4517	1.8665	0.2698
G*N	-0.7434	0.1207	-1.8139	-0.0166	0.6959	-0.1274	2.3813	-0.8975
N*N	-0.1060	0.0413	-0.2302	0.4085	-0.3078	0.6065	-0.9022	0.4754
R*R	-0.7777	-0.1857	0.0111	-0.9435	-1.9291	-0.9566	-0.6372	1.3498
G*G	-0.2616	-0.6096	-1.2937	-0.7039	-1.2663	-0.8549	-0.5070	0.6869
NDVI	0.0934	0.5357	-0.0367	-0.2997	-0.2591	-0.4956	0.3120	1.7667

	min	mean	max	rms	PSNR
W2 stats	0.0000	0.0214	0.7347	0.0389	28.1923

Figure 4.9: Blue is a linear combination in bitants of all bands from figure 2.3

4.9 B(N,R,G)—bitant split

Red and green channel from the CIR photo in figure 2.3, page 9. Blue is generated from a linear combination of the near-infrared, red, and green channels.

The regression was carried out in two domains defined by having $NDVI > 0$ (vegetation) and $NDVI < 0$ (non-vegetation).

The PSNR is 0.45 dB lower than in the $B = \mathrm{B}(N,R,G)$ octant case (section 4.6) and 0.35 dB higher than the plain $B = \mathrm{B}(N,R,G)$ case (section 4.3). There is, however, no visible difference between this case and the $B = \mathrm{B}(N,R,G)$ octant case.

```
     no veg   vegetation
WH =
N   -0.0174   -0.1973
R    0.5117    0.1451
G    0.2733    0.8322

           min      mean     max       rms      PSNR
WH stats  0.0000   0.0321   0.7197   0.0492   26.1523
```

Figure 4.10: Blue is a linear combination in bitants of all bands from figure 2.3

4.10 B(N,R,G,NDVI)—bitant split

Red and green channel from the CIR photo in figure 2.3, page 9. Blue is generated from a linear combination of the near-infrared, red, and green channels, combined with the NDVI based on the red and near-infrared channels.

The regression was carried out in two domains defined by having $NDVI > 0$ (vegetation) and $NDVI < 0$ (non-vegetation).

The PSNR is 1.2 dB lower than in the $B = \mathrm{B}(N,R,G,NDVI)$ octant case (section 4.7) and 0.4 dB higher than the plain $B = \mathrm{B}(N,R,G,NDVI)$ case (section 4.4). There is, however, no visible difference between this case and the $B = \mathrm{B}(N,R,G)$ octant case.

```
        no veg   vegetation
WI =
N      -0.0073   -0.2138
R       0.4018    0.2553
G       0.2124    0.6970
NDVI    0.1370    0.0425

           min      mean     max       rms      PSNR
WI stats  0.0000   0.0269   0.6788   0.0467   26.6061
```

Figure 4.11: Blue is a linear combination in bitants of all bands from figure 2.3

4.11 B(R,G,NDVI)—bitant split

Red and green channel from the CIR photo in figure 2.3, page 9. Blue is generated from a linear combination of the near-infrared, red, and green bands of the original CIR photo. combined with the NDVI based on the red and near-infrared channels.

The regression was carried out in two domains defined by having $NDVI > 0$ (vegetation) and $NDVI < 0$ (non-vegetation).

The PSNR is 1.2 dB lower than in the $B = \mathrm{B}(N, R, G, NDVI)$ octant case (section 4.5) and 1.2 dB higher than the plain $B = \mathrm{B}(R, G, NDVI)$ case (section 4.4). There is, however, no visible difference between this case and the $B = \mathrm{B}(N, R, G)$ octant case.

```
     no veg   vegetation
WJ =
R       0.4102    0.0651
G       0.1936    0.7301
NDVI    0.1376    0.0413

           min       mean      max       rms       PSNR
WJ stats  0.0000   0.0272   0.7051   0.0471   26.5393
```

Chapter 5

Discussion and conclusion

Let us briefly reiterate the objectives and expectations of this work (cf. chapter 1),

> ... the main objective of this work is to *compute a number of linear transforms for deriving an artificial blue channel in suburban areas, and to investigate the relative merits of those transforms*.
>
> The *a priori* expectation is that a minor extension to the simple $blue = 0$ scheme will take us a long way, and that computationally more expensive approaches adds minor gains only.

By and large, the *a priori* expectation was fulfilled: the $B = \mathrm{B}(N,R,G)$ case (section 4.3) improves dramatically on the plain $B = 0$ case (section 4.1), and significantly on the $B = \mathrm{B}(R,G)$ case (section 4.2).

Including NDVI into the regression gave a very slight visual improvement, but the octant and bitant split experiments did not result in any further visual improvement.

This, combined with the much more complex and computationally expensive setup for the computation of the octant/bitant blue channel synthesis (cf. appendix D), makes it an obvious recommendation to use the $B = \mathrm{B}(N,R,G)$, although the $B = \mathrm{B}(N,R,G,NDVI)$ model might be used if NDVI is already computed for use in subsequent processing steps.

If all aerial photography was carried out in 4 channel digital form, this work would have been unnecessary.

Calibrated photogrammetric cameras for aerial photography are, however, still much more common than 4 channel digital aerial sensor systems. Until that changes, some kind of transformation from colour-infrared to true colours is still quite useful for presentation purposes. The work presented here represents the first approximation to such a transformation for use in suburban areas. The approximation is derived using a simple linear least squares method. More physically correct methods could have been applied if all details in the photographic chain were known—which they frequently are not. In this setting, we go for a further improvement based on heuristics, which is the subject of ongoing work.

For now, use of the model

$$B = -0.14 \times N + 0.24 \times R + 0.70 \times G$$

is recommended as a first guess.

Bibliography

Vlad C. Cardei. From dichromatic to trichromatic images; implications for image recovery and visualization. In *Proceedings of the Image Processing, Image Quality, Image Capture Systems Conference (PICS '99), April 25-28, 1999, Savannah, Georgia*, page 5, 1999.

Robert E. Crippen. Calculating the vegetation index faster. *Remote Sensing of Environment*, 34:71–73, 1990.

Thomas Knudsen, editor. *Proceedings of the seminar on remote sensing and image analysis techniques for revision of topographic databases*, National Survey and Cadastre—Denmark, Technical Report no. 13, Copenhagen, Denmark, 2000. National Survey and Cadastre—Denmark. ISBN 87-7866-227-3.

Thomas Knudsen, John Kamper, Henning Skriver, Rune C. Andersen, Karsten Engsager, and Ole Andersen. The joint KMS/DCRS demo CDROM: An invitation for collaborative change detection studies. In Knudsen (2000), pages 95–98. ISBN 87-7866-227-3.

Thomas Knudsen and Brian P. Olsen. Automated change detection for updates of digital map databases. *Photogrammetric Engineering & Remote Sensing*, 2003. Accepted for publication oct. 2002.

Thomas Knudsen and Brian Pilemann Olsen. Detection of buildings in aerial photos for semi-automated revision of map databases. *International Archives of Photogrammetry, Remote Sensing and Spatial Information Sciences*, XXXIV(3B):120–125, 2002.

Kodak. *KODAK AEROCHROME III Infrared Film 1443, KODAK AEROCHROME III Infrared NP Film SO-734, KODAK Publication No. AS-77*. Eastman Kodak Company, November 2002. URL `http://www.kodak.com/country/US/en/government/aerial/technicalPubs/tiDocs/ti2562/ti2562.shtml`.

Bettina Petzold. Revision of topographic databases by satellite images—experiences and expectations. In Knudsen (2000), pages 15–23. ISBN 87-7866-227-3.

Bettina Petzold and Volker Walter. Revision of topographic databases by satellite images. In Manfred Schroeder, Karsten Jacobsen, Gottfried Konecny, and Christian Heipke, editors, *Sensors and mapping from space 1999*, page 9, Hanover, Germany, 1999. ISPRS.

Volker Walter. The design and implementation of an automated system for revision of topographic databases. In Knudsen (2000), pages 7–14. ISBN 87-7866-227-3.

Appendix A

The Kodak 1443 colour-infrared film

Figure A.1 (reproduced from Kodak (2002)) shows the spectral sensitivity for the three wavebands in Kodak 1443 film.

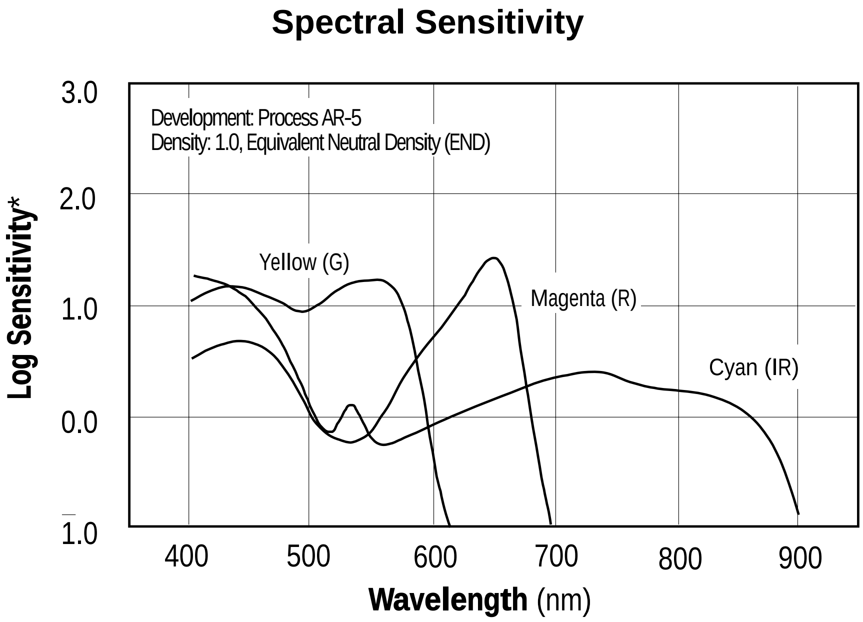

Figure A.1: Kodak 1443 channel sensitivity (reproduced from Kodak (2002))

Note the high sensitivity for the high-energetic blue photons in all bands. This is taken care of by mounting a yellow (= minus blue) filter in front of the aerial photogrammetric camera, so blue light is entirely excluded from the colour-infrared imaging process.

The colour formation process in colour-infrared photography is outlined in figure 1.1, page 5.

Appendix B

The ADAR 5500 airborne sensor system

The ADAR 5500 data were picked up from URL `http://www2.oneonta.edu/~baumanpr/ncge/highres/hartford/`, and were originally provided for use (almost) without restriction by Positive Systems, Inc., of Whitefish, Montana. The text included below is the "readme" file provided with the data.

```
--------------------------------------------------------------------------------

 ADAR SYSTEM 5500 IMAGERY
             ~Urban Landscape in Connecticut - FULL SIZED SCENE~

This "coastal" scene was captured near Hartford, Connecticut  USA.  This image
was used to generate a GIS basemap, map water impervious/pervious surfaces,
and identify diseased vegetation.

This image was captured by the ADAR System 5500 at a resolution of approximately
0.5 meter per pixel.  The following GPS information was captured for the aircraft
at the time this image was taken:  Latitude = 41.573166 Deg Deg. N , Longitude =
72.640476 Deg. W, heading = 272 Deg. TN, and the date was Sat May  1, 1999  17:57:12
Greenwich Mean Time (GMT).  The spectral band information for this scene is as
follows:

     Band Center         Wavelength/Bandwidth (nm)                Color
     Band 1                450-515                    Blue
     Band 2                525-605                    Green
     Band 3                630-690                    Red
     Band 4                750-900                    Near IR

Image dimensions are: 966 ROWS by 1493 COLUMNS.


This scene is provided free of charge by Positive Systems, Inc. This image data
may be used without restriction for education, research, or publication as long
as proper credit is given to Positive Systems as the source of the image data.
This image data may be copied and shared as long as the recipient receives all
associated data files (including this "readme" file).

For more information on this imagery or any ADAR Systems, contact

Positive Systems
250 Second Street East
Whitefish, MT  59937  USA
phone:      (406) 862-7745
fax:        (406) 862-7759
email:      positive@possys.com
internet:   www.possys.com

--------------------------------------------------------------------------------
```

Evidently, the center wavelengths of the ADAR 5500 red and green bands run quite close to the center wavelengths of the corresponding Kodak 1443 bands (appendix A), while the near-infrared sensitivities vary more widely. In cases of more detailed modelling, this could be taken into account. There are, however, numerous other factors (developer details, scanner setup) influencing the spectral response of the final digitized aerial photo. In this study such details are deliberately left out.

Appendix C

Summary of numerical results

	min	mean	max	rms	PSNR	channels used	domain
W0	0.0000	0.2801	1.0000	0.3321	9.5751	(none)	full
WB	0.0000	0.0725	0.7594	0.0979	20.1879	R, G	full
WC	0.0000	0.0360	0.6881	0.0513	25.7982	N, R, G	full
WE	0.0000	0.0305	0.6581	0.0490	26.2038	N, R, G, NDVI	full
W1	0.0000	0.0357	0.6684	0.0540	25.3583	R, G, NDVI	full
WF	0.0000	0.0301	0.6706	0.0468	26.5924	N, R, G	octant
WG	0.0000	0.0240	0.7108	0.0409	27.7721	N, R, G, NDVI	octant
W2	0.0000	0.0214	0.7347	0.0389	28.1923	(see below)	octant
WH	0.0000	0.0321	0.7197	0.0492	26.1523	N, R, G	veg/noveg
WI	0.0000	0.0269	0.6788	0.0467	26.6061	N, R, G, NDVI	veg/noveg
WJ	0.0000	0.0272	0.7051	0.0471	26.5393	R, G, NDVI	veg/noveg

Channels used for W2: N, R, G, NR, RG, GN, NN, RR, GG, NDVI

channel		N	R	G	NDVI
W0	=	[0	0	0	0]'
WB	=	[0.0000	0.1757	0.4430	0.0000]'
WC	=	[-0.1423	0.2415	0.7007	0.0000]'
WE	=	[-0.1248	0.3018	0.5683	0.0612]'
W1	=	[0.0000	0.4528	0.3024	0.0801]'

WF =

octant	0	1	2	3	4	5	6	7
N	-0.1357	0.0336	-0.4949	0.0185	-0.2250	-0.1249	-0.2704	-0.2654
R	0.0755	0.5058	0.5392	0.1383	0.7801	0.5494	0.1163	0.4559
G	0.8755	0.1589	0.6562	0.5893	0.2533	0.3406	0.8638	0.6217

WG =

octant	0	1	2	3	4	5	6	7
N	-0.0742	0.0377	-0.5012	0.0102	-0.1321	-0.1612	-0.2711	-0.1894
R	0.3932	0.3775	0.5534	0.1796	0.5982	0.7421	0.1114	0.7137
G	0.3849	0.1246	0.6611	0.6213	0.1865	0.3964	0.8639	0.8037
NDVI	0.0992	0.1512	-0.0128	-0.0666	0.1537	-0.2220	0.0054	-0.7213

W2 =

octant	0	1	2	3	4	5	6	7
N	0.1589	0.0457	1.3731	-0.5297	-0.0757	-1.0522	0.5289	0.3732
R	0.3393	-0.4199	-0.2935	1.1845	1.3166	1.2913	0.5662	-2.5408
G	0.3375	0.0690	0.1773	0.4259	0.4075	1.3465	-0.6154	0.0836
N*R	-0.1046	0.0487	-1.6563	-0.1005	-1.1329	0.1757	-2.3948	0.3172
R*G	1.5717	1.5754	3.8368	1.2009	2.5794	0.4517	1.8665	0.2698
G*N	-0.7434	0.1207	-1.8139	-0.0166	0.6959	-0.1274	2.3813	-0.8975
N*N	-0.1060	0.0413	-0.2302	0.4085	-0.3078	0.6065	-0.9022	0.4754
R*R	-0.7777	-0.1857	0.0111	-0.9435	-1.9291	-0.9566	-0.6372	1.3498
G*G	-0.2616	-0.6096	-1.2937	-0.7039	-1.2663	-0.8549	-0.5070	0.6869
NDVI	0.0934	0.5357	-0.0367	-0.2997	-0.2591	-0.4956	0.3120	1.7667

WH =

	no veg	vegetation
N	-0.0174	-0.1973
R	0.5117	0.1451
G	0.2733	0.8322

WI =

	no veg	vegetation
N	-0.0073	-0.2138
R	0.4018	0.2553
G	0.2124	0.6970
NDVI	0.1370	0.0425

WJ =

	no veg	vegetation
R	0.4102	0.0651
G	0.1936	0.7301
NDVI	0.1376	0.0413

Appendix D

Source code

The source code for model fitting and blue channel synthesis is reproduced below. The code is written in Matlab and intended for informational purposes only: It is not production quality code—rather a set of plumbings for semi-automated generation of the results presented in this report.

Please bear in mind that the results generated from this code is intended as a “decent first guess” only. This first guess is to be used as input to a subsequent set of heuristic transformations, which will be presented in a forthcomming publication.

Tests have been carried out on a Sun Ultra-4 running Matlab version 6.5.0.180913a, release 13 under Solaris 7 (aka SunOS 5.7).

Links to the electronic form of the source code are available on URL `http://research.kms.dk/~thk/pubs/`

D.1 Model Fitting

```
%%%%%%%%%%%%%%%%%%%%%%%%%%%%%%%%%%%%%%%%%%%%%%%%%%%%%%%%%%%%%%%%%%%%%%%%%%%%%%%
%
%               P  S  E  U  D  O  T  R  U  E  _  F  I  T   .    M
%
%   matlab functions for fitting pseudo-true colour models from 4 channel data
%
%   Thomas Knudsen, thk@kms.dk - 2003-03
%
%%%%%%%%%%%%%%%%%%%%%%%%%%%%%%%%%%%%%%%%%%%%%%%%%%%%%%%%%%%%%%%%%%%%%%%%%%%%%%%


function [dummy] = pseudotrue_fit(dummy)

% determine linear transformation for pseudo-true colours


%------------------------------------------------------------------------------

% AREA1 image - R,G,B
A=imread('AREA1/AREA1_9324.png');
R = reshape((double(A(:,:,1))/255.),[],1);
G = reshape((double(A(:,:,2))/255.),[],1);
B = reshape((double(A(:,:,3))/255.),[],1);

WA = [R G]\B
BB = [R G]*WA;
[mn, me, mx, rms, psnr] = erdsc(B,BB,1,'WA (from plain rgb)  ');
moo = [mn, me, mx, rms, psnr];

clear A  R  G  B BB; pack;

%------------------------------------------------------------------------------




% hartford image - near infrared channel
A=imread('hartford/sphar_ir.pgm');

% the matrix idx helps mask out the water covered areas of the hartford image
row = repmat((1:size(A,1))', 1, size(A,2));
```

```
col = repmat((1:size(A,2)),  size(A,1), 1);
idx = col-row;

N = (double(A)/255.);
% generate a masked image for illustrative purposes
M=N;
M(idx>500)=0;
imwrite(M, 'mask.png');
n = N(idx<500);
n = reshape(n, [],1);
N = reshape(N, [],1);

% hartford image - red channel
A=imread('hartford/sphar_rd.pgm');
R = (double(A)/255.);
r = R(idx<500);
r = reshape(r, [],1);
R = reshape(R, [],1);

% hartford image - green channel
A=imread('hartford/sphar_gr.pgm');
G = (double(A)/255.);
g = G(idx<500);
g = reshape(g, [],1);
G = reshape(G, [],1);

% hartford image - blue channel
A=imread('hartford/sphar_bl.pgm');
B = (double(A)/255.);
b = B(idx<500);
b = reshape(b, [],1);
B = reshape(B, [],1);


%------------------------------------------------------------------------------


%
% octant number for each pixel in (N,R,G)-space
%
O = (N>0.5) + 2 * (R > 0.5) + 4 * (G > 0.5);
OO = reshape(uint8(32 * O), [size(A)]);
imwrite(OO,'sphar_cir-octant.png');

NO(1) = size(O(O==0),1);
NO(2) = size(O(O==1),1);
NO(3) = size(O(O==2),1);
NO(4) = size(O(O==3),1);
NO(5) = size(O(O==4),1);
NO(6) = size(O(O==5),1);
NO(7) = size(O(O==6),1);
NO(8) = size(O(O==7),1);

prod(size(O))
NO * 100.0 ./ prod(size(O))


%------------------------------------------------------------------------------


P =  R./(N+R+1e-6);  % IPVI, (1e-6 to avoid div by zero)
p =  r./(n+r+1e-6);  % IPVI, (1e-6 to avoid div by zero)

%------------------------------------------------------------------------------


W0 = [0 0 0]'
BB = [N R G]*W0;
[mn, me, mx, rms, psnr] = erdsc(B,BB,1,'W0 (no blues)  ');
moo = [moo; mn, me, mx, rms, psnr];

WB = [0; WA]
BB = [N R G]*WB;
[mn, me, mx, rms, psnr] = erdsc(B,BB,1,'WB (WA used on Hartford)  ');
moo = [moo; mn, me, mx, rms, psnr];

WC = [N R G]\B
BB = [N R G]*WC;
[mn, me, mx, rms, psnr] = erdsc(B,BB,1,'WC (from all pixels)  ');
moo = [moo; mn, me, mx, rms, psnr];

WD = [n r g]\b
bb = [n r g]*WD;
[mn, me, mx, rms, psnr] = erdsc(b,bb,1,'WD (from land pixels)  ');
moo = [moo; mn, me, mx, rms, psnr];
```

```
WE = [N R G P]\B
BB = [N R G P]*WE;
[mn, me, mx, rms, psnr] = erdsc(B,BB,1,’WE (from N,R,G,NDVI)  ’);
moo = [moo; mn, me, mx, rms, psnr];

W1 = [R G P]\B
BB = [R G P]*W1;
[mn, me, mx, rms, psnr] = erdsc(B,BB,1,’W1 (from R,G,NDVI)  ’);
moo = [moo; mn, me, mx, rms, psnr];

W2 = domain_fit([N,R,G,N.*R,R.*G,G.*N,N.^2,R.^2, G.^2,P],B,O)
BB = domain_synth([N,R,G,N.*R,R.*G,G.*N,N.^2,R.^2, G.^2,P],O, W2);
[mn, me, mx, rms, psnr] = erdsc(B,BB,1,’W2 (from N,R,G,NR,RG,GN,NN,RR,GG,NDVI)  ’);
moo = [moo; mn, me, mx, rms, psnr];

WF = domain_fit([N,R,G],B,O)
BB = domain_synth([N,R,G],O, WF);
[mn, me, mx, rms, psnr] = erdsc(B,BB,1,’WF (from octant N,R,G)  ’);
moo = [moo; mn, me, mx, rms, psnr];


WG = domain_fit([N,R,G,P],B,O)
BB = domain_synth([N,R,G,P],O, WG);
[mn, me, mx, rms, psnr] = erdsc(B,BB,1,’WG (from octant N,R,G,NDVI)  ’);
moo = [moo; mn, me, mx, rms, psnr];


O = zeros(size(P));
O(P>0.1) = 1;
O(P>0.2) = 2;
O(P>0.3) = 3;
O(P>0.4) = 4;
O(P>0.5) = 5;
O(P>0.6) = 6;
O(P>0.7) = 7;
O(P>0.8) = 8;
O(P>0.9) = 9;

W3 = domain_fit([N,R,G,N.*R,R.*G,G.*N,N.^2,R.^2, G.^2,P],B,O)
BB = domain_synth([N,R,G,N.*R,R.*G,G.*N,N.^2,R.^2, G.^2,P],O, W3);
[mn, me, mx, rms, psnr] = erdsc(B,BB,1,’W3 (from N,R,G,NR,RG,GN,NN,RR,GG,NDVI)  ’);
moo = [moo; mn, me, mx, rms, psnr];

O = zeros(size(P));
O(P>0.5) = 1;
OO = reshape(uint8(255 * O), [size(A)]);

imwrite(OO,’sphar_cir-ndvimask.png’);
WH = domain_fit([N R G],B,O)
BB = domain_synth([N R G],O, WH);
[mn, me, mx, rms, psnr] = erdsc(B,BB,1,’WH (from vegmasked N,R,G)  ’);
moo = [moo; mn, me, mx, rms, psnr];

WI = domain_fit([N R G P],B,O)
BB = domain_synth([N R G P],O, WI);
[mn, me, mx, rms, psnr] = erdsc(B,BB,1,’WI (from vegmasked N,R,G,NDVI)  ’);
moo = [moo; mn, me, mx, rms, psnr];

WJ = domain_fit([R G P],B,O)
BB = domain_synth([R G P],O, WJ);
[mn, me, mx, rms, psnr] = erdsc(B,BB,1,’WJ (from vegmasked R,G,NDVI)  ’);
moo = [moo; mn, me, mx, rms, psnr];

clear   A   n r g b bb p    N R G B   BB P
clear   O M NO OO  col row idx  me mn mx psnr rms dummy ans; pack

ti = datestr(now);
save weights.mat

dummy=1



%-------------------------------------------------
%    set of error descriptors
%-------------------------------------------------
function [mn, me, mx, rms, psnr] = erdsc(B, BB, prt, prefix);
peaksig = 1;
%peaksig = max(B);
mn     =   min(abs(BB-B));
me     =   mean(abs(BB-B));
mx     =   max(abs(BB-B));
rms    =   sqrt(sum((BB-B).^2)/prod(size(B)));
psnr   =   20*log10(peaksig/(sqrt(mean((BB-B).^2))));
```

```
rlmx   =   max(abs(25500*(BB-B)./(255*B+1)));
if prt==1,
disp(sprintf([prefix '%6.4f   %6.4f   %6.4f   %6.4f   %6.4f'], [mn me mx rms psnr]));
end;





%-------------------------------------------------
%    multi domain fitting
%-------------------------------------------------
function [MM] = domain_fit(NRG,B,D);
BB = B;
for I = 0:max(D),
    nrg = NRG(D==I,:);
    b = B(D==I);
    M = nrg\b;
    if (I==0), MM = M; else MM = [MM M]; end;
    bb = nrg * M;
    BB(D==I) = bb;
    [mn, me, mx, rms, psnr] = erdsc(B, BB, 1, [int2str(I) '(' int2str(max(D)) ')   ']);
end;
return



%-------------------------------------------------
%    multi domain synthesis
%-------------------------------------------------
function [BB] = domain_synth(NRG,D, MM);
BB = zeros(size(D));
for I = 0:max(D),
    nrg = NRG(D==I,:);
    M = MM(:,I+1);
    bb = nrg * M;
    BB(D==I) = bb;
end;
return
```

D.2 Blue Channel Synthesis

```
%%%%%%%%%%%%%%%%%%%%%%%%%%%%%%%%%%%%%%%%%%%%%%%%%%%%%%%%%%%%%%%%%%%%%%%%%%%%%%%
%
%         P  S  E  U  D  O  T  R  U  E  _  S  Y  N  T  H    .     M
%
%    matlab functions for synthesis of pseudo-true colours from colour-infrared
%    aerial photos.
%
%   Thomas Knudsen, thk@kms.dk - 2003-03
%
%%%%%%%%%%%%%%%%%%%%%%%%%%%%%%%%%%%%%%%%%%%%%%%%%%%%%%%%%%%%%%%%%%%%%%%%%%%%%%%


function [dummy] = pseudotrue_synth(dummy)

% cwd /data/GEK/topop/EXPERIMENTS/RGB-NIR/hartford

% determine linear transformation for pseudo-true colours


%------------------------------------------------------------------------------

load weights.mat
disp('dummy');dummy
%------------------------------------------------------------------------------

if dummy==1,
% AREA1 image - CIR
A = imread('AREA1/AREA1_4563.png');
f = 'AREA1-';
s = size(A);
N = reshape((double(A(:,:,1))/255.),[],1);
R = reshape((double(A(:,:,2))/255.),[],1);
G = reshape((double(A(:,:,3))/255.),[],1);

% octant number for each pixel in (N,R,G)-space
O = (N>0.5) + 2 * (R > 0.5) + 4 * (G > 0.5);
OO = reshape(uint8(32 * O), size(A(:,:,1)));
imwrite(OO,'AREA1_4563-octant.png');

%------------------------------------------------------------------------------
```

```
elseif dummy==2,
% AREA2 image - CIR
A = imread('AREA2/AREA2_4563.png');
f = 'AREA2-';
s = size(A);
N = reshape((double(A(:,:,1))/255.),[],1);
R = reshape((double(A(:,:,2))/255.),[],1);
G = reshape((double(A(:,:,3))/255.),[],1);

% octant number for each pixel in (N,R,G)-space
O = (N>0.5) + 2 * (R > 0.5) + 4 * (G > 0.5);
OO = reshape(uint8(32 * O), size(A(:,:,1)));
imwrite(OO,'AREA2_4563-octant.png');

%--------------------------------------------------------------------------------

elseif dummy==3,
% AREA2 image - CIR
A = imread('2002-05-18/tr20.ppm');
f = 'tr20-';
s = size(A);
N = reshape((double(A(:,:,1))/255.),[],1);
R = reshape((double(A(:,:,2))/255.),[],1);
G = reshape((double(A(:,:,3))/255.),[],1);

% octant number for each pixel in (N,R,G)-space
O = (N>0.5) + 2 * (R > 0.5) + 4 * (G > 0.5);
OO = reshape(uint8(32 * O), size(A(:,:,1)));
imwrite(OO,'tr20-octant.png');

%--------------------------------------------------------------------------------
else
disp('pseudotrue_synth: bad value for dummy'); dummy
return
end



NO(1) = size(O(O==0),1);
NO(2) = size(O(O==1),1);
NO(3) = size(O(O==2),1);
NO(4) = size(O(O==3),1);
NO(5) = size(O(O==4),1);
NO(6) = size(O(O==5),1);
NO(7) = size(O(O==6),1);
NO(8) = size(O(O==7),1);

prod(size(O))
NO * 100.0 ./ prod(size(O))


%--------------------------------------------------------------------------------

P =  R./(N+R+1e-6);  % IPVI, (1e-6 to avoid div by zero)

%--------------------------------------------------------------------------------


BB = [N R G]*WB; B=BB;
imwrite(reshape([R G BB], s), [f 'WB.jpg']);

BB = [N R G]*WC;
imwrite(reshape([R G BB], s), [f 'WC.jpg']);
disp('C'); [mean(abs(B-BB)) mean(abs(R./(2+BB)))]

BB = [N R G P]*WE;
imwrite(reshape([R G BB], s), [f 'WE.jpg']);
disp('E'); [mean(abs(B-BB)) mean(abs(R./(2+BB)))]

BB = [R G P]*W1;
imwrite(reshape([R G BB], s), [f 'W1.jpg']);
disp('1'); [mean(abs(B-BB)) mean(abs(R./(2+BB)))]

BB = domain_synth([N,R,G,N.*R,R.*G,G.*N,N.^2,R.^2, G.^2,P],O, W2);
imwrite(reshape([R G BB], s), [f 'W2.jpg']);
disp('2'); [mean(abs(B-BB)) mean(abs(R./(2+BB)))]



BB = domain_synth([N R G], O, WF);
imwrite(reshape([R G BB], s), [f 'WF.jpg']);
disp('F'); [mean(abs(B-BB)) mean(abs(R./(2+BB)))]

BB = domain_synth([N R G P], O, WG);
```

```
imwrite(reshape([R G BB], s), [f 'WG.jpg']);
disp('G'); [mean(abs(B-BB)) mean(abs(R./(2+BB)))]

O = zeros(size(P));
O(P>0.1) = 1;
O(P>0.2) = 2;
O(P>0.3) = 3;
O(P>0.4) = 4;
O(P>0.5) = 5;
O(P>0.6) = 6;
O(P>0.7) = 7;
O(P>0.8) = 8;
O(P>0.9) = 9;

BB = domain_synth([N,R,G,N.*R,R.*G,G.*N,N.^2,R.^2, G.^2,P],O, W3);
imwrite(reshape([R G BB], s), [f 'W3.jpg']);
disp('3'); [mean(abs(B-BB)) mean(abs(R./(2+BB)))]

O = zeros(size(P));
O(P>0.5) = 1;
OO = reshape(uint8(255 * O), [size(A(:,:,1))]);
NO(1) = size(O(O==0),1);
NO(2) = size(O(O==1),1);
prod(size(O))
NO * 100.0 ./ prod(size(O))


BB = domain_synth([N R G],O, WH);
imwrite(reshape([R G BB], s), [f 'WH.jpg']);
disp('H'); [mean(abs(B-BB)) mean(abs(R./(2+BB)))]

BB = domain_synth([N R G P],O, WI);
imwrite(reshape([R G BB], s), [f 'WI.jpg']);
disp('I'); [mean(abs(B-BB)) mean(abs(R./(2+BB)))]

BB = domain_synth([R G P],O, WJ);
imwrite(reshape([R G BB], s), [f 'WJ.jpg']);
disp('J'); [mean(abs(B-BB)) mean(abs(R./(2+BB)))]

clear all; pack;



%-------------------------------------------------
%    set of error descriptors
%-------------------------------------------------
function [mn, me, mx, rms, psnr] = erdsc(B, BB, prt, prefix);
peaksig = 1;
%peaksig = max(B);
mn     =   min(abs(BB-B));
me     =   mean(abs(BB-B));
mx     =   max(abs(BB-B));
rms    =   sqrt(sum((BB-B).^2)/prod(size(B)));
psnr   =   20*log10(peaksig/(sqrt(mean((BB-B).^2))));
rlmx   =   max(abs(25500*(BB-B)./(255*B+1)));
if prt==1,
disp(sprintf([prefix '%6.4f   %6.4f   %6.4f   %6.4f   %6.4f'], [mn me mx rms psnr]));
end;



%-------------------------------------------------
%    multi domain fitting
%-------------------------------------------------
function [MM] = domain_fit(NRG,B,D);
BB = B;
for I = 0:max(D),
    nrg = NRG(D==I,:);
    b = B(D==I);
    M = nrg\b;
    if (I==0), MM = M; else MM = [MM M]; end;
    bb = nrg * M;
    BB(D==I) = bb;
```

```
    [mn, me, mx, rms, psnr] = erdsc(B, BB, 1, [int2str(I) '(' int2str(max(D)) ')   ']);
end;
return



%-------------------------------------------------
%    multi domain synthesis
%-------------------------------------------------
function [BB] = domain_synth(NRG,D, MM);
BB = zeros(size(D));
for I = 0:max(D),
    nrg = NRG(D==I,:);
    M = MM(:,I+1);
    bb = nrg * M;
    BB(D==I) = bb;
end;
return
```

Technical Report Series

The National Survey and Cadastre—Denmark, Technical Report series is intended as an informal report series, published at irregular intervals. The following reports have so far been published in the series (up to number 3, the reports were named "Geodætisk Institut, Technical Reports", from number 4 through 7, the reports were named "National Survey and Cadastre—Denmark, Geodetic Division, Technical Reports").

1. Jørgen Eeg: *On the Adjustment of Observations in the Presence of Blunders*, 32 pp., 1986
2. Per Knudsen, C.C. Tscherning and René Forsberg: *Gravity Field Mapping Around the Faeroe Islands and Rockall Bank from Satellite Altimetry and Gravimetry*, 30 pp., 1987
3. Niels Andersen: *The Structure and Filling of a 19.2 Kilometer Hydrostatic Leveling Tube*, 83 pp., 1988
4. René Forsberg: *Gravity Measurements in East Greenland 1986-1988*, 32 pp., 1991
5. Gabriel Strykowski: *Automation Strategy for Repeated Tasks in DOS*, 15 pp., 1992
6. Simon Ekholm and Kristian Keller: *Gravity and GPS Survey on the Summit of the Greenland Ice Sheet 1991-1992*, 26 pp., 1993
7. Per Knudsen: *Integrated Inversion of Gravity Data*, 52 pp., 1993
8. Thomas Knudsen: *Geophysical Use of Geographical Information Systems*, 76 pp., 1996
9. Simon Ekholm: *Determination of Greenland Surface Topography from Satellite Altimetry and Other Elevation Data*, 23 pp., 1997
10. René Forsberg, Arne Olesen and Kristian Keller: *Airborne Gravity Survey of the North Greenland Shelf 1998*, 34 pp., 1999
11. Cecilia S. Nielsen: *Topography and Surface Velocities of an Irregular Ice Cap in Greenland Assessed by the means of GPS, Laser Altimetry and SAR Interferometry*, 81 pp., 2001
12. Cecilia S. Nielsen: *Estimation of Ice Topography and Surface Velocities Using SAR Interferometry*, 37 pp., 2001
13. Thomas Knudsen (ed): *Proceedings of the seminar on remote sensing and image analysis techniques for revision of topographic databases, Copenhagen, Denmark 2000-02-29*, 119 pp., 2000
14. Lars Brodersen: *Maps as Communication - Theory and Methodology in Cartography*, 88 pp., 2001
15. Claus V. Petersen og Simon Ekholm: *Analyse af digitale terrænmodeller beregnet fra satellitbåren SAR interferometri, Case studies af udvalgte områder i Grønland og Danmark*, 20 pp., 2001
16. Olwijn Leeuwenburgh: *Combined Analysis of Sea Surface Height and Temperature for Mapping and Climate Studies*, 96 pp., 2001
17. Calin Arens: *Some examples of topographic applications and accuracy of laser scanning*, 66 pp, 2002
18. René Forsberg, Arne V. Olesen, Kristian Keller and Mads Møller: *Airborne Gravity Survey of Sea Areas Around Greenland and Svalbard 1999-2001*, 55pp., 2002
19. Jacob L. Høyer: *On the Combination of Satellite and In Situ Observations to Detect Oceanic Processes*, 115 pp., 2002
20. Thomas Knudsen: *Linear mappings for "true" colour presentation of suburban colour-infrared aerial photos*, 35 pp., 2003
21. René. Forsberg, Kristian Keller, Sine M. Hvidegård and Arne Olesen: *ESAG-2002: European airborne gravity and lidar survey in the Arctic Ocean*, 28 pp., 2003
22. René Forsberg, Arne Olesen: *Airborne gravity survey of the Foxe Basin, Nunavut*, 13 pp., 2003
23. P. Knudsen, O.B. Andersen, T. Knudsen, O. Leeuwenburgh, J. L. Høyer, A. A.Nielsen, K. B. Hilger, C. C. Tscherning, N. K. Højerslev, G. Moreaux, E. Buch og V. Huess: *Geoid and Sea Level of the North Atlantic Region—GEOSONAR—Final Report*, 40 pp, 2003.

Reports may be ordered from the individual authors at the adress
Kort & Matrikelstyrelsen, Rentemestervej 8, DK-2400 Copenhagen NV, Denmark
URL: `http://www.kms.dk` `http://research.kms.dk`